ZEAXANTHIN RADICAL CATION FORMATION IN MINOR LIGHT-HARVESTING COMPLEXES OF HIGHER PLANT ANTENNA

[2,3†]Avenson, T.J., [1,2†]Ahn, T.K., [1,2]Zigmantas, D., [1,3]Niyogi, K.K., [1,3]Li, Z. [4]Ballottari, M., [4]Bassi, R., and [1,2*]Fleming, G.R.

[1]Physical Biosciences Division, Lawrence Berkeley National Laboratory, Berkeley, CA 94720
[2]Department of Chemistry, Hildebrand B77, University of California, Berkeley, CA 94720-1460
[3]Department of Plant and Microbial Biology, 111 Koshland Hall, University of California, Berkeley, CA 94720-3102
[4]Department of Science and Technology, University of Verona, Italy 37134

Running head: zeaxanthin radical cation formation

[*]To whom correspondence should be addressed: e-mail: GRFleming@lbl.gov; tel.: 510-643-3944; fax: 510-643-7012

[†]These authors contributed equally to this work.

Previous work on intact thylakoid membranes showed that transient formation of a zeaxanthin radical cation was correlated with regulation of photosynthetic light harvesting via energy-dependent quenching. A molecular mechanism for such quenching was proposed to involve charge transfer within a chlorophyll-zeaxanthin heterodimer. Using near infrared (880-1100 nm) transient absorption spectroscopy, we demonstrate that carotenoid (mainly zeaxanthin) radical cation generation occurs solely in isolated minor light-harvesting complexes that bind zeaxanthin, consistent with the engagement of charge transfer quenching therein. We estimated that less than 0.5% of the isolated minor complexes undergo charge transfer quenching *in vitro*, whereas the fraction of minor complexes estimated to be engaged in charge transfer quenching in isolated thylakoids was more than 80 times higher. We conclude that minor complexes which bind zeaxanthin are sites of charge transfer quenching *in vivo* and that they can assume Non-quenching and Quenching conformations, the equilibrium LHC(N)↔LHC(Q) of which is modulated by the transthylakoid pH gradient, the PsbS protein, and protein-protein interactions.

INTRODUCTION

Higher plant photosynthesis is initiated by absorption of light in pigment-binding (antenna) proteins that transfer absorbed solar energy to the reaction centers of photosystems (PS) II and I where energy conversion begins (1). The PSII-associated light-harvesting complexes (LHCs) bind chlorophylls and carotenoids that are involved in both the harvesting and transfer of energy to the reaction center, and the harmless dissipation of excitation energy in excess of photosynthetic capacity (2). Thus, the PSII LHCs are critical 'branch-points' for energy partitioning during photosynthesis. The peripheral antenna consists of trimeric complexes composed of LHCII proteins, the major LHC of higher plant antennae. In between the peripheral LHCII and the reaction center there are three 'minor' LHCs referred to as CP29, CP26, and CP24 (1).

Dissipation of excess light energy during photosynthesis involves several photoprotective mechanisms which are collectively referred to as non-photochemical quenching (NPQ) (2,3). The predominant component of NPQ is referred to as energy dependent quenching, or qE, and it is rapidly reversible and correlated with zeaxanthin (Z) formation (4). Mutants of *A. thaliana* have been instrumental in confirming the involvement of Z (5) and identifying a role for PsbS in qE (6). The *npq*4 mutant lacks a functional PsbS protein and exhibits very little qE (6). The PsbS protein has been subsequently proposed to be involved in controlling qE by sensing thylakoid lumen pH (7). The xanthophyll cycle consists of the enzymatic and reversible conversion of the thylakoid-associated pigment violaxanthin (V) to antheraxanthin (A) to Z (8). Very little qE is exhibited in the *A. thaliana* mutant referred to as *npq1* which is impaired in its ability to convert V to Z as a result of a lesion in the gene encoding the thylakoid lumen-localized enzyme violaxanthin de-epoxidase (5). Conversely, the *npq2* mutant of *A. thaliana* constitutively accumulates Z and lacks V and neoxanthin due to a lesion in the gene encoding Z epoxidase (5).

Elucidating the molecular details of qE has proved to be a major challenge. An approach involving computational modeling (9-11), molecular genetics (5,6), biochemistry (12) and ultrafast laser spectroscopy (13,14) led to a proposed molecular mechanism for qE based on analyses of a semi-intact system (thylakoids) (13). Quantum chemical calculations indicated that the lowest energy, excited singlet state of a chlorophyll-zeaxanthin heterodimer ([Chl-Z]), for separations of ≤ ~5Å, was a charge transfer (CT) state involving essentially complete transfer of an electron from Z to chlorophyll (9,10). These findings led to a proposed CT quenching model for the molecular mechanism of qE in which the [Chl-Z] quenches chlorophyll singlet excited states, thereby transiently producing zeaxanthin radical cations ($Z^{\bullet+}$) (9,10).

Femtosecond transient absorption (TA) spectroscopy of isolated spinach thylakoids in the near infrared region (NIR) demonstrated transient evolution of a $Car^{\bullet+}$ in an qE-dependent manner (13). The NIR TA kinetics from isolated thylakoids of various mutants of *A. thaliana* specifically impaired in qE, including the *npq1* and the *npq*4 mutants, did not show transient $Car^{\bullet+}$ formation (13). Transient $Car^{\bullet+}$ signals in *npq2* and *npq2lut2*, a mutant that constitutively accumulates Z but also lacks lutein, were very similar to each other (13). These results, along with the spectral signature (13), imply that the $Car^{\bullet+}$ transiently formed in the wild type thylakoids is a $Z^{\bullet+}$ species. The quenching of *bulk* chlorophyll by transfer of energy to a [Chl-Z] quenching complex that undergoes charge separation and subsequent recombination to the ground state provides a simple model for qE (13).

Initiation of qE invokes a conformational change of at least one of the LHCs, triggered by contributions from ΔpH, PsbS, and Z (15). This implies that an equilibrium exists between non-quenching (N) and quenching (Q) forms: LHC(N) ↔ LHC(Q). Indeed the presence of distinct N and Q conformations in detergent solution has been reported on the basis of spectroscopic measurements (16,17) and confirmed by biochemical methods (18). At low light (i.e. in the absence of significant ΔpH, Z, etc.), the equilibrium must lie well to the left (non-quenching form). However, if Z becomes a major xanthophyll that is present, it is possible that a small fraction of the complexes are in the LHC(Q) configuration and may be detectable, *e.g.* Z alone can shift the equilibrium somewhat to the right. In this paper, we present evidence using the $Z^{\bullet+}$ signal as a diagnostic that this is indeed the case for the minor LHCs (CP24, CP26, and CP29). Using the $Z^{\bullet+}$ signature to infer CT quenching, we estimate that ~80 times more of the minor complexes undergo CT quenching in thylakoids engaged in steady-state qE in comparison to isolated complexes. Taken together our results are suggestive of the minor complexes being sites of CT quenching *in vivo*.

MATERIALS AND METHODS

Isolation of antenna LHCs with specific xanthophylls

Unstacked thylakoids were isolated from leaves of dark-adapted wild type, conditions under which V accumulates, and *npq*2 strains of *A. thaliana* as previously described (19). Solubilized samples were then fractionated by ultracentrifugation in a 0.1 to 1 M sucrose gradient containing 0.06% α-DM and 10 mM HEPES at a pH of 7.5 (22 h at 280,000 g, 4°C). This procedure yields distinct bands from which monomeric (Band 2) and trimeric LHCII (Band 3) complexes can be separated (18). SDS-PAGE analysis of Bands 2 and 3 from dark-adapted wild type and *npq*2 mutant strains was performed with a Tris-Tricine buffer system as described in (20). Pigments were extracted from the isolated antenna complexes with 80% acetone, then separated and quantified by HPLC as described in (21) and by fitting analysis of the spectrum of the acetone extract with the spectra of individual pigments as described in (22). Trimeric LHCII and monomeric complexes were re-suspended in buffer solution (5 mM HEPES and 0.06% α-DM at pH 7.6) to an OD of ~0.3/mm (all samples were adjusted to the same O.D. at 650 nm) and ~0.05/cm at 650 nm for TA and time-resolved fluorescence analyses, respectively. The genes for the three monomeric LHCII polypeptides (Lhcb 1-3) were individually expressed in *E. coli*, the apoproteins were isolated, followed by *in vitro* re-constitution with chlorophylls (*a* and *b*) and either V or Z.

NIR transient absorbance

The NIR TA laser system has been previously described (13). Briefly, the repetition rate was 250 kHz and the pump pulses were tuned to ~650 nm (i.e. the chlorophyll *b* Q_y transition). The maximum pump energy and FWHM of the pulse auto-correlation trace were ~48 nJ/pulse and ~40 fs, respectively. We chose 650 nm as our excitation wavelength because the output power of our OPA was higher than that at 680 nm, yielding higher signal:noise ratios. Chlorophyll *b* to *a* energy transfer occurs on the 100-200 fs and tens of ps timescale (23), making results on the timescale studied here insensitive to whether chlorophyll *b* or chlorophyll *a* is initially excited. White light continuum probe pulses were generated in a 1 mm quartz plate. The observation of the cross-correlation function of the pump and probe overlap was ca. 85 fs. The diameters of the pump and probe beams at the sample holder were 141 μm and 81 μm, respectively. The mutual polarizations of the pump and probe beams were set to the magic angle (54.7°). The time resolution of our TA measurements was 5ps/point (-60 ps to -10 ps), 0.5 ps/point (-10 ps to 60 ps), and 5 ps/point (65 ps to 600 ps). A monochromator (Spectra Pro 300i, Acton Research Corp., Acton, MA) with a spectral resolution of 2.7 nm and a InGaAs photodiode (DET410, Thorlabs, Newton, NJ) was used to monitor transmission. A sample cell for isolated LHCs with a path length of 1 mm was chilled by a circulating water bath (VWR Scientific 1160, PolyScientific, Niles, IL) which was set at 7°C during the data acquisition to prevent sample degradation. The path length of the cuvette used for isolated thylakoids was 2 mm and was continuously translated (0.2 Hz) during experiments to avoid sample degradation.

Measurements of fluorescence lifetimes

Time-resolved fluorescence was detected using a time-correlated single photon counting (TCSPC) technique. A Ti:sapphire oscillator (1.1 W at 910 nm, 76 MHz Coherent MIRA 900) pumped an optical parametric oscillator (Coherent MIRA OPO). Output pulses with 110 mW average power at 1300 nm were frequency doubled in a 1 mm BBO crystal to generate 650 nm pulses with an average power of ~7 mW. Using a home-made pulse picker driven by a RF frequency generator (CAMAC CD 1000), the repetition rate of the excitation laser beam was reduced to 3.8 MHz. Fluorescence signals were detected by a temperature controlled microchannel plate photomultiplier (Hamamatsu, R2809U-01) and amplified by a preamplifier (Becker & Hickl GmbH, HFAC-26dB). Triggering pulses were obtained by partial reflection of the excitation beam with a silicon photodiode (Newport, 818-BB-20) and a 1 GHz preamplifier (EG&G ORTEC, 9306). A personal computer with a TCSPC module (Becker and Hickl GmbH, SPC-600) was used for data collection and processing. The resulting instrument function had a FWHM of ~40 ps. The timing card for our TCSPC set up possessed 6.1 ps/channel resolution. The maximum amplitude of the signals was greater than 15,000-20,000 counts.

PAM chlorophyll *a* fluorescence of isolated thylakoids

A pulsed amplitude modulated (PAM) chlorophyll *a* fluorimeter, as described in (13), was used to measure modulated fluorescence in intact, stacked *A. thaliana* thylakoids that were isolated as in (13).

RESULTS

Isolation of PSII LHCs containing specific xanthophyll species

Our aim was to determine whether CT quenching could be supported in isolated LHCs with specific xanthophyll compositions. Figure 1 shows SDS-PAGE analysis of whole thylakoids (Lane A) and Bands 2 (monomeric complexes) and 3 (trimeric LHCII complexes) from dark-adapted wild type (Lanes B and C) and *npq*2 (Lanes D and E) strains. Band 2 from both wild type and *npq*2 consist of all three minor complexes as well the all three monomeric isoforms of LHCII (Lhcbs 1-3). Band 3 from *npq*2 and wild type proved to be trimeric LHCII. We could not detect PsbS in Bands 2 and 3 from either wild type or *npq*2 (data not shown).

The LHCs isolated from dark-adapted wild type and *npq*2 are expected to be specifically enriched in V and Z, respectively. We performed HPLC to analyze the xanthophyll content of Bands 2 and 3 of *npq*2 and wild type strains (Table 1). Consistent with the *npq*2 phenotype, Band 2 (monomers) from this strain possessed 9.3 Z

molecules per 100 chlorophylls, whereas A and V were not detected. Conversely, Band 2 from dark-adapted wild type thylakoids exhibited no detectable Z/A, while there were 5.2 V molecules per 100 chlorophylls. LHCII trimeric complexes (Band 3) from wild type and *npq*2 strains contained no detectable Z and 6.6 Z molecules/100 chlorophylls, respectively. These data are consistent with the LHCs isolated from dark-adapted wild type and *npq*2 strains binding V and Z, respectively. The LHCs isolated from dark-adapted wild type thylakoids are referred to throughout as MLHC-V (Monomeric LHCs enriched with V) and LHCII-V (trimeric LHCII complexes binding V), whereas the complexes isolated from *npq2* thylakoids are referred to as MLHC-Z (monomeric LHCs that bind Z) and LHCII-Z (trimeric LHCII complexes that bind Z).

Evidence for transient $Z^{\bullet+}$ formation solely in minor complexes

To explore whether or not $Car^{\bullet+}$ formation could be supported in isolated LHCII and MLHC complexes, NIR TA kinetic traces were measured by photoexcitation of the monomeric (Figure 2A) and LHCII trimeric (Figure 2B) complexes at 650 nm. The MLHC-V NIR TA kinetic profile at 1000 nm (black trace) exhibited two decay components with time constants of 60 ps and 1087 ps (Table 2). These pure decay features (i.e. no slow rise component) originate solely from chlorophyll excited state absorbance (ESA) dynamics (13) and are therefore inconsistent with $Car^{\bullet+}$ formation.

Similarly, the LHCII-V and LHCII-Z TA traces at 1000 nm exhibit bi-exponential decays without any rise component (Figure 2B), consistent with recent observations (24), yielding time constants of 43 ps and 799 ps for LHCII-V complexes and 67 ps and 954 ps for the counterparts that bind Z (Table 3). These pure decay kinetics in LHCII correspond to chlorophyll ESA dynamics, rather than transient $Car^{\bullet+}$ formation, even when LHCII binds Z. To explore the slight differences between the NIR TA traces of the LHCII-V and LHCII-Z complexes, we generated a difference kinetic trace (blue curve) and found differences which were of the same amplitude as the noise level before time zero. Furthermore, the convoluted rise time constant (~50 ps) seems to be equal to the fastest decay components of the LHCII-V or –Z kinetics, which likely originates from a slight difference in chlorophyll ESA, or singlet-singlet annihilation, between the two types of complexes.

In contrast , the 1000 nm TA kinetic of the MLHC-Z sample (Figure 2A, red trace) shows a small rise component with a time constant of 2.9 ps (the amplitude was less than 5%), followed by bi-exponential decay of 69 ps and 358 ps (Table 2). The differences between the MLHC-V and MLHC-Z kinetics are emphasized in the difference profile (Figure 2A, blue trace) that was obtained by subtracting the MLHC-V TA kinetic from that of the MLHC-Z complexes. The NIR TA difference profile was characterized by 5.2 ps and 238 ps rise and decay components, respectively (Table 2). The time constants of the difference profile from the MLHCs are comparable to those of the corresponding rise and decay time constants of the difference TA kinetics acquired using isolated thylakoids, providing evidence for CT quenching in isolated complexes (13). The differences between the MLHCs and thylakoids in the rise and decay time constants may reflect differences in the dynamics of singlet-singlet annihilation and influences of the protein environment on charge recombination within the [Chl-Z] complex.

The MLHC-Z sample contains several monomeric complexes (Figure 1) from which the $Car^{\bullet+}$ signal could originate. Figure 3 shows NIR TA kinetics for all three of the individual LHCII monomers that were re-constituted *in vitro* with either V or Z (Table 4). Whether bound by Z or V, the TA kinetics for all three LHCII monomers correspond solely to decay dynamics, inconsistent with $Car^{\bullet+}$ formation in these complexes. These combined results imply that the transient $Car^{\bullet+}$ signal observed in the MLHC-Z sample most likely originates within the minor complexes that bind Z.

The $Car^{\bullet+}$ species observed in the MLHC-Z sample could be either a lutein radical cation ($Lut^{\bullet+}$) or a $Z^{\bullet+}$ (Table 1). Figure 4 shows a TA spectrum that was reconstructed from the maximum amplitude (i.e. at ~15 ps) of the NIR TA difference profiles that were obtained from 880-1080 nm. The spectrum exhibits broad absorption with a peak centered at ~980 nm (Figure 4), a blue-shift of ~20 nm relative to the $Z^{\bullet+}$ spectrum

previously obtained in spinach thylakoids (13), possibly representing species-dependent differences in $Z^{\bullet+}$ absorption. However, the peak of the $Z^{\bullet+}$ spectrum was recently shown to be centered at ~980 nm (24). Therefore, these results imply that the observed transient $Car^{\bullet+}$ signal in the MLHC-Z sample represents $Z^{\bullet+}$ formation. Nonetheless, since the MLHC-V and MLHC-Z samples contain 11.5 lutein molecules/100 chlorophylls (Table 1), an alternative interpretation is that the observed $Car^{\bullet+}$ signal is a $Lut^{\bullet+}$. The spectrum of the $Lut^{\bullet+}$ peaks at ~920 and ~950 nm depending upon the solvent used (25-27), and has recently also been reported to peak at 880 nm (24), significantly blue-shifted relative to the peak of the spectrum in Figure 4. We can not exclude the possibility that a small $Lut^{\bullet+}$ signal is present on the blue shoulder of the $Z^{\bullet+}$ spectrum. Therefore, we conclude that the observed transient $Car^{\bullet+}$ signal is *mainly* due to $Z^{\bullet+}$ formation specifically in minor complexes that bind Z, consistent with CT quenching of chlorophyll excited states therein.

Z-dependent quenching of chlorophyll excited states in isolated antennae LHCs

To obtain direct information about the quenching of chlorophyll excited states, chlorophyll *a* fluorescence quantum yields were estimated using time-correlated single photon counting (TCSPC). Figure 5 shows the fluorescence decay profiles for MLHC and LHCII (Panels A and B, respectively) complexes. The amplitude of a 0.63 ns component increased from 8.8% in the MLHC-V complexes (Panel A) to 22.8% in the corresponding MLHCs that were shown to bind Z (Table 5). The amplitude of a 2.18 ns component was 27% and 32.9% in the MLHC-V and MLHC-Z complexes, respectively. A 5 ps component indicative of CT quenching (Figure 2A, blue trace) was not observed in the fluorescence kinetics. Convolutions using our instrument response function demonstrated that unless a 5 ps component was greater than 10% (data not shown), it would not be observable, implying that very few of the MLHC-Z complexes assume the CT quenching configuration when isolated from the intact system. The fluorescence quantum yield in the MLHC-Z complexes was estimated to be 18% lower than that of MLHC-V.

The fluorescence kinetics of the LHCII trimeric complexes (Figure 5B) also exhibited multi-exponential decay (Table 6). An increase in a 2.5 ns component from 30.7% to 55.5% and a concomitant decrease in the amplitude of a 3.9 ns component accounts for the 11% lower fluorescence quantum yield in the LHCII-Z complexes relative to LHCII-V complexes. These data demonstrate Z-dependent quenching of chlorophyll excited states in LHCII, essentially as has been previously reported (18,28), presumably by a mechanism other than CT quenching. Two possible mechanisms include transfer of energy either to the S_1 state of Z (29,30) or to an excitonically coupled chlorophyll-pair energy trap (31,32).

Comparable NIR TA and PAM fluorescence analyses of thylakoids

In order to explore CT quenching in an intact system, NIR TA kinetics were obtained in thylakoids engaged in qE. Figure 6 shows NIR TA kinetics obtained by excitation of isolated *A. thaliana* thylakoids at 650 nm and probing at 1000 nm. The NIR TA kinetics measured in the thylakoids under steady-state actinic illumination at ~500 μmol photons m^{-2} s^{-1} (Figure 6A, red trace), conditions that result in the conversion of V to Z, were dominated by a single component with a time constant of 134 ps (100% amplitude) (Table 7). It should be pointed out that a rise component, similar to that observed in the MLHC-Z kinetic (Figure 2A, red trace) which exhibited a 2.9 ps time constant, is likely not resolvable given the noise level of our thylakoid data. The NIR TA profile obtained ~10 minutes post-actinic illumination (Figure 6A, black trace) could be fit using two decay components with time constants of 10 ps (43% amplitude) and 134 ps (58% amplitude) (Table 7). A difference profile was constructed by subtracting the TA kinetics that were obtained after the light-dark transition from those obtained under steady-state illumination and was characterized by single exponential rise and decay components with time constants of 10 ps and 133 ps, respectively (Table 7), very similar to previous observations (13). The NIR TA kinetics were measured under conditions in which the PSII reaction centers remain variably open, *e.g.* the rate constant for photochemistry (k_P) assumes a non-zero value.

To compare the NIR TA kinetics from thylakoids with estimates of qE that also take into consideration non-zero values for k_P, we adapted a recently introduced convention (33,34) for expressing the fraction of photons dissipated by qE, or quantum yield of qE (Φ_{qE}). Figure 6 (inset) shows a modulated fluorescence trace for dark-adapted thylakoids exposed to ~500 μmol photons m^{-2} s^{-1}. The maximum yields of modulated fluorescence under steady-state (i.e. actinic) illumination (Fm') and 10 minutes following a light-dark transition (Fm") were estimated upon application of a saturating flash (>10,000 μmol photons m^{-2} s^{-1}) as in (35), whereas the steady-state yield of fluorescence (Fs) was acquired under actinic illumination without a saturating flash. The Φ_{qE} was expressed as:

$$\Phi_{qE} = [(Fm" - Fm')/Fm"] * (Fs/Fm') \qquad (1)$$

where the modulated fluorescence parameters are defined in terms of rate constants as $Fm' = k_f/(k_f + k_{ISC} + k_{IC} + k_{qE} + k_{qT} + k_{qI})$, $Fs = k_f/(k_f + k_{ISC} + k_{IC} + k_{qE} + k_{qT} + k_{qI} + k_P)$, and $Fm" = k_f/(k_f + k_{ISC} + k_{IC} + k_{qI} + k_{qT})$. Rate constants other than k_{qE}, k_{qT}, and k_{qI} (i.e. the rate constants for qE, state transitions, and the slowly recovering component of NPQ referred to as qI, respectively) are defined according to (33,34). An estimate of ~0.43 was obtained for Φ_{qE} under the same conditions that $Z^{\bullet+}$ formation was measured.

Comparison of CT quenching in isolated LHCs and thylakoids

To compare the extent of CT quenching within the isolated MLHC-Z complexes with that in thylakoids engaged in qE, we determined the concentration of excited minor complexes ($MIcomp^*$) and the $[Z^{\bullet+}]$ within what we refer to as the probe volume (RV) (i.e. the volume in which complexes are excited by the laser beam and within which $Z^{\bullet+}$ formation is probed). The RV was approximated by a cylinder as determined by the spot size of the probe beam at the sample and the width of the sample cuvette. The number of $MIcomp^*$ within the RV was derived from the chlorophyll *a*/*b* ratios of the MLHC-Z and thylakoid samples, which were based, in part, on ODs at ~650 nm of ~0.30 and ~0.50, respectively (data not shown). The $[Z^{\bullet+}]$ within the RV of the MLHC and thylakoid samples was obtained from the maximum amplitude of the difference NIR TA profiles (Figures 2A and 6B, blue traces) and an extinction coefficient of 8000 $M^{-1}cm^{-1}$ for $Z^{\bullet+}$ as reported in (36).

An estimate of 1.13 x 10^{10} $MIcomp^*$ was obtained for the MLHC-Z sample. Since the minor LHCs isolated from the *npq*2 mutant bind 1 Z per complex (18), the fraction of MIcomp* undergoing CT quenching was estimated as:

$$[Z^{\bullet+}]/MIcomp* \qquad (2)$$

Using an OD of ~1.2 x 10^{-5} for the $Z^{\bullet+}$ in the *npq*2 monomeric sample, 4.7 x 10^7 $Z^{\bullet+}$ species were estimated within the RV. According to Eqn. 2, ~0.42% of the MIcomp* were approximated to be undergoing CT quenching, an analysis that is consistent with the model in which the equilibrium MLHC(N) ↔ MLHC(Q) is shifted predominantly, although not completely, to the left. We suggest that the slight shift of the equilibrium to the right is mediated simply by binding of Z to the isolated complexes.

Similarly, we obtained a value of 1.09 x 10^{10} $MIcomp^*$ within the RV for the isolated thylakoids. Since each minor complex in isolated thylakoids binds on average 0.33 Z per monomer (37) (i.e. fewer than that of the minor complexes isolated from the *npq*2 mutant) we estimated, using an OD of 5.85 x 10^{-4} for $Z^{\bullet+}$ formation, 2.33 x 10^9 $Z^{\bullet+}$ within the RV. In order to take into consideration the dynamics of energy transfer within the thylakoid membrane, and to express the *limits* of CT quenching in the minor complexes (as estimated according to Eqn. 2), the approximations for CT quenching in thylakoids took into account singlet-singlet annihilation (i.e. by assuming a range of percentages of the complexes were doubly excited and subtracting off this fraction from the total number of MIcomp*) in the minor complexes and excitation energy transfer (EET) from LHCII to a CT quenching site within the minor complexes.

Figure 7 demonstrates that CT quenching within all three minor complexes can account for the magnitude of the estimates of Φ_{qE} (the horizontal, hatched bar represents our 43 ±5% estimate of Φ_{qE} in isolated thylakoids) if EET from LHCII to a quenching site within the minor

complexes is between ~20-50% and singlet-singlet annihilation within the minor complexes is between 0-50%. Importantly, within the uncertainty of these estimates, the fraction of minor complexes undergoing CT quenching was 80 to 100 times higher in thylakoids compared to isolated minor complexes, consistent with the equilibrium MLHC(N) ↔ MLHC(Q) being shifted significantly to the right in the intact system.

DISCUSSION

Our results and those of our earlier work demonstrate that $Z^{\bullet+}$ formation in isolated thylakoid membranes correlates positively with all phenomena (i.e. Z, PsbS, ΔpH etc.) that distinguish qE from the other components (i.e. qI, etc.) of NPQ (13). It might, therefore, seem unlikely that this key signature of qE would be observable in isolated, Z-bound LHCs where no pH gradient or PsbS is present. The absence of a $Car^{\bullet+}$ signal in isolated, LHCII trimeric complexes that were shown to bind Z (Figure 2B) seems to support this point of view, although it should be pointed out that it remains possible that CT quenching could be engaged in LHCII trimers *in vivo*. It is quite striking, therefore, that the data from a mixture of monomeric complexes shows clear evidence for transient $Car^{\bullet+}$ formation (Figure 2A) when Z replaces V within the complexes (Table 1), implying that the $Car^{\bullet+}$ species formed is specifically a $Z^{\bullet+}$. The $Z^{\bullet+}$ signal putatively originates within one or more of the minor complexes (CP29, CP26 and CP24), suggesting that the CT mechanism of quenching might occur within these sites *in vivo*. Without experiments on pure samples of the individual minor complexes, it is not yet possible to say whether the $Z^{\bullet+}$ signal is associated specifically with only one of the minor complexes or with more than one of them. Analysis of *A. thaliana* mutants suggest that none of the minor complexes is a unique site of qE *in vivo*. Antisense plants that specifically lack CP29 or CP26 exhibit little effect on qE (38), whereas depletion of CP24 was recently shown to decrease (but not eliminate) qE due to a perturbation of the PSII antenna structure (39). The minor complexes are believed to occupy a position in the bulk antennae between the LHCII periphery and the reaction center (40,41). Dekker and Boekema (42) have suggested that energy transfer from LHCIIs in the PSII supercomplex may flow through the minor complexes to reach the PSII core, and that excitation energy from CP24 may flow through CP29 to reach the core. The placement of three minor complexes between the moderately/strongly bound LHCII trimers and the PSII core (see Fig 4 of ref. (42)) means that the presence of a quenching site in the minor complexes should be highly effective in preventing over excitation of the reaction center, one of the proposed roles of qE (3,43).

We estimate that less than ~1% of the excited minor complexes in the MLHC-Z sample undergo CT quenching. These results are consistent with the need for protein-protein interactions in the native membrane (15), combined with the ΔpH and protonated PsbS (2,13,44), to shift the equilibrium MLHC-Z(N)↔MLHC-Z(Q) significantly to the right, a notion that is supported by the observed ~80-fold increase in the fraction of minor complexes that were estimated to be undergoing CT quenching in thylakoids engaged in steady-state qE (Figure 6).

The very small fraction of isolated MLHC-Z complexes able to mediate CT quenching is consistent with our fluorescence decay measurements. Tests showed that we could detect a 5 ps component, *e.g.* the timescale of $Z^{\bullet+}$ formation that is indicative of CT quenching (Figure 2A), in our time-resolved fluorescence profiles if it accounted for 10% or more of the decay, and in fact no such component could be detected (Figure 5; Table 5).

One of the implications of this work is that NPQ is highly heterogeneous, both in its molecular mechanisms and its sites in the antenna of PSII, issues currently under debate in the literature (2,13,44). Our results suggest that the minor complexes serve as sites of CT quenching during qE. Experiments in which individual chlorophyll molecules are successively removed from the MLHC-Z complex should be valuable in pinning down the molecular mechanism of the transition between non-quenching and quenching states since the energy of the CT state of [Chl-Z] dimers depends sensitively on the separation and orientation of the two molecules (10,11). We found no evidence for CT quenching (Figure 6, inset) during engagement of the slowly recovering component of NPQ referred to as 'qI-type' quenching in isolated thylakoids, implying that it

occurs via an alternative molecular mechanism(s), several possibilities for which have appeared in the literature (15,31,32). qI-type quenching does not depend on ΔpH and PsbS, whereas, like qE it has been suggested to require Z (4,18). In fact, quenching of chlorophyll excited states within isolated (i.e. no PsbS and ΔpH) minor complexes that bind Z has been previously observed and ascribed to qI-type quenching (18), consistent with the longer time-scale (>0.5 ns) quenching in our TCSPC data representing this qI-type quenching. A model in which the minor complexes facilitate both qE and qI-types of quenching by employing different molecular mechanisms, both of which are modulated by the physiology of the photosynthetic membrane, may help to reconcile much of the current controversy concerning the molecular mechanisms and sites of the various components of NPQ in the PSII super complex.

CONCLUSIONS

Our results strongly suggest that minor LHCs (CP24, CP26 and CP29) provide sites for CT quenching, a mechanism for dissipating chlorophyll singlet excited states that was previously shown to correlate specifically with qE (13). The minor complexes are well positioned to dissipate excess absorbed energy in PSII. Experiments using individual complexes may further pinpoint the precise location of CT quenching in PSII, as well as the nature of the presumed conformational transition required to turn 'on' or 'off' the CT mechanism.

Acknowledgements

We would like to thank Dr. Y.C. Cheng for many helpful discussions and simulations. R.B. extends thanks to the FIRB contract RBLA0345SF from the Italian Basic Research Foundation and contract SAMBA Trento Research Council for foundational support. This work was also supported by the Korea Research Foundation Grant (KRF- 2006-214- C00037) funded by the Korean Government (MOEHRD) (T.K.A.), the National Research Initiative Competitive Grant (2006-03279) (T.J.A.), and by the Office of Basic Energy Sciences, Chemical Sciences Division, U.S. Department of Energy (contract DE-AC02-05CH11231 (G.R.F. and K.K.N).

REFERENCES

1. Green, B. R., and Durnford, D. G. (1996) *Annu. Rev. Plant Physiol. Plant Mol .Biol.* **47**, 685-714
2. Horton, P., Ruban, A. V., and Walters, R. G. (1996) *Annu. Rev. Plant Physiol. Plant Mol .Biol.* **47**, 655-684
3. Muller, P., Li, X. P., and Niyogi, K. K. (2001) *Plant Physiol* **125**, 1558-1566
4. Demmig-Adams, B. (1990) *Biochim. Biophys. Acta*, 1-24
5. Niyogi, K. K., Grossman, A. R., and Bjorkman, O. (1998) *Plant Cell* **10**, 1121-1134
6. Li, X. P., Bjorkman, O., Shih, C., Grossman, A. R., Rosenquist, M., Jansson, S., and Niyogi, K. K. (2000) *Nature* **403**, 391-395
7. Li, X. P., Gilmore, A. M., Caffarri, S., Bassi, R., Golan, T., Kramer, D., and Niyogi, K. K. (2004) *J. Biol. Chem.* **279**, 22866-22874
8. Yamamoto, H. Y., Nakayama, T. O., and Chichester, C. O. (1962) *Arch. Biochem. Biophys.* **97**, 168-173
9. Dreuw, A., Fleming, G. R., and Head-Gordon, M. (2003) *Phys. Chem. Chem. Phys.* **5**, 3247-3256
10. Dreuw, A., Fleming, G. R., and Head-Gordon, M. (2005) *Biochem. Soc. Trans.* **33**, 858-862
11. Dreuw, A., and Head-Gordon, M. (2004) *J. Am. Chem. Soc.* **126**, 4007-4016
12. Gilmore, A. M., Hazlett, T. L., and Govindjee. (1995) *Proc. Natl. Acad. Sci. U S A* **92**, 2273-2277
13. Holt, N. E., Zigmantas, D., Valkunas, L., Li, X. P., Niyogi, K. K., and Fleming, G. R. (2005) *Science* **307**, 433-436

14. Ma, Y. Z., Holt, N. E., Li, X. P., Niyogi, K. K., and Fleming, G. R. (2003) *Proc. Natl. Acad. Sci. U S A* **100**, 4377-4382
15. Horton, P., Wentworth, M., and Ruban, A. (2005) *FEBS Lett.* **579**, 4201-4206
16. Crimi, M., Dorra, D., Bosinger, C. S., Giuffra, E., Holzwarth, A. R., and Bassi, R. (2001) *Eur. J. Biochem.* **268**, 260-267
17. Moya, I., Silvestri, M., Vallon, O., Cinque, G., and Bassi, R. (2001) *Biochemistry* **40**, 12552-12561
18. Dall'Osto, L., Caffarri, S., and Bassi, R. (2005) *Plant Cell* **17**, 1217-1232
19. Bassi, R., Hoyer-Hansen, G., Barbato, R., Giacometti, G. M., and Simpson, D. J. (1987) *J. Biol. Chem.* **262**, 13333-13341
20. Schagger, H., and von Jagow, g. (1987) *Anal. Biochem.* **166**, 368-379
21. Gilmore, A. M., and Yamamoto, H. Y. (1991) *Plant Physiol* **96**, 635-643
22. Croce, R., Canino, G., Ros, F., and Bassi, R. (2002) *Biochemistry* **41**, 7334-7343
23. Croce, R., Muller, M. G., Bassi, R., and Holzwarth, A. R. (2003) *Biophys. J.* **84**, 2508-2516
24. Amare, S., Standfuss, J., Barros, T., Kulbrandt, W., Dreuw, A., and Wachtveitl, J. (2007) *J Phys. Chem. B* **111**, 3481-3487
25. Edge, R., Land, E. J., McGarvey, D., Mulroy, L., and Truscott, T. G. (1998) *J. Am. Chem. Soc.* **120**, 4087-4090
26. Galinato, M. G., Niedzwiedzki, D., Deal, C., Birge, R. R., and Frank, H. A. (2007) *Photosynth. Res.* **94**, 67-78
27. Mortensen, A., and Skibsted, L. H. (1997) *J. Food Chem.* **1997**, 2970-2977
28. Polivka, T., Zigmantas, D., Sundstrom, V., Formaggio, E., Cinque, G., and Bassi, R. (2002) *Biochemistry* **41**, 439-450
29. Demmig-Adams, B., Gilmore, A. M., and Adams, W. W. (1996) *FASEB J.* **10**, 403-412
30. Frank, H. A., Cua, A., Chynwat, V., Young, A., Gosztola, D., and Wasielewski, M. R. (1994) *Photosynth. Res.* **41**, 389-395
31. Liu, Z., Yan, H., Wang, K., Kuang, T., Zhang, J., Gui, L., An, X., and Chang, W. (2004) *Nature* **428**, 287-292
32. Pascal, A. A., Liu, Z., Broess, K., van Oort, B., van Amerongen, H., Wang, C., Horton, P., Robert, B., Chang, W., and Ruban, A. (2005) *Nature* **436**, 134-137
33. Hendrickson, L., Forster, B., Pogson, B. J., and Chow, W. S. (2005) *Photosynth. Res.* **84**, 43-49
34. Hendrickson, L., Furbank, R. T., and Chow, W. S. (2004) *Photosynth. Res.* **82**, 73-81
35. Avenson, T. J., Cruz, J. A., and Kramer, D. M. (2004) *Proc. Natl. Acad. Sci. U S A* **101**, 5530-5535
36. Han, R.-M., Tain, Y.-X., Wu, Y.-S., Wang, P., Ai, X.-C., Zhang, J.-P., and Skibsted, L. H. (2006) *Photochem. Photobiol. Sci.* **82**, 538-546
37. Morosinotto, T., Baronio, R., and Bassi, R. (2002) *J. Biol. Chem.* **277**, 36913-36920
38. Andersson, J., Walters, R. G., Horton, P., and Jansson, S. (2001) *Plant Cell* **13**, 1193-1204
39. Kovacs, L., Damkjaer, J., Kereiche, S., Ilioaia, C., Ruban, A. V., Boekema, E. J., Jansson, S., and Horton, P. (2006) *Plant Cell* **18**, 3106-3120
40. Bassi, R., and Dainese, P. (1992) *Eur. J. Biochem.* **204**, 317-326
41. Harrer, R., Bassi, R., Testi, M. G., and Schafer, C. (1998) *Eur. J. Biochem.* **255**, 196-205
42. Dekker, J. P., and Boekema, E. J. (2005) *Biochim. Biophys. Acta* **1706**, 12-39

43. Holt, N. E., Fleming, G. R., and Niyogi, K. K. (2004) *Biochemistry* **43**, 8281-8289
44. Horton, P., and Ruban, A. (2005) *J. Exp. Bot.* **56**, 365-373
45. Tracewell, C. A., and Brudvig, G. W. (2003) *Biochemistry* **42**, 9127-9136

FIGURE LEGENDS

Figure 1. SDS-PAGE analysis of thylakoids and isolated LHCs from *A. thaliana* wild type and *npq2*. The isolated bands purified from sucrose gradients and thylakoids were loaded on a SDS-PAGE gel using Tris-Tricine buffer system in order to asses the protein composition. Bands corresponding to CP29, CP26, CP24, Lhcb1+Lhcb2, and Lhcb3 were detected in the thylakoids and Band 2 from wild type and *npq*2, while bands from Lhcb1+Lhcb2 and Lhcb3 are the only traces detected in Band 3.
Lane 1: molecular weight marker (Mw), Lane A: thylakoids from wild type *A.t.*, Lane B: Band 2 from wild type, Lane C: Band 3 from wild type, Lane D: Band 2 from *npq2*, Lane E: Band 3 from *npq2*.

Figure 2. NIR TA profiles for isolated LHCs. NIR TA profiles were estimated using monomeric (Panel A) and LHCII trimeric (Panel B) complexes. The red and black profiles represent TA kinetics for the corresponding complexes bound by Z and V, respectively, and represent an average of more than 10 kinetic sweeps. It should be noted that these kinetics have not been normalized in any way. Difference kinetic traces (blue) correspond to subtraction of the V-kinetic profiles from the Z-kinetics.

Figure 3. NIR TA kinetics of individual Z- and V-bound LHCII monomeric complexes. NIR TA kinetics were obtained for Lhcb1 (Panel A), Lhcb2 (Panel B), and Lhcb3 (Panel C) that were isolated from *E. coli* in which the genes for the individual complexes had been transformed. The respective LHCII monomeric complexes were reconstituted in the presence of chlorophylls (*a* and *b*) and either the xanthophyll species Z (red traces) or V (black traces). Experiments were carried out by excitation of the complexes at 650 nm and probing at 980 nm. Each trace is an average of more then 10 kinetic sweeps.

Figure 4. Transient carotenoid radical cation spectrum of isolated monomeric complexes. A range of NIR TA kinetics were generated in isolated monomeric complexes that bind either V or Z by probing from 880-1080 nm. Reconstructed TA difference profiles were generated and a spectrum (blue trace) was reconstructed by estimating the maximum amplitude of the difference profiles (i.e. average of time-points 13-17 ps) at ~15 ps. Shown for comparison is the solution spectrum (black dashed line) of the β carotene radical cation (45). Error bars represent the standard error (SE) of the mean of 5 time-points.

Figure 5. Fluorescence lifetime estimates of isolated LHCs. Fluorescence lifetime estimates of monomeric (MLHCs) (panel A) and LHCII trimeric (Panel B) complexes were obtained using time-correlated single photon counting by excitation of the samples at 650 nm and detection of chlorophyll fluorescence at 690 nm. The corresponding complexes shown to bind Z and V are represented by red and black traces, respectively. The maximum number of counts at the maximum amplitude of the kinetics was between 15,000-20,000.

Figure 6. NIR TA kinetics in isolated thylakoids under qE conditions. Estimates of qE (inset) were obtained in isolated thylakoids of wild type *A. thaliana*, as described in text, using a PAM fluorimeter as in (13). NIR TA profiles (Panel A) were measured under steady-state actinic illumination (~400 μmol photons $m^{-2}s^{-1}$) (red trace) and several minutes after transition to darkness (black trace) by excitation of the thylakoids at 650 nm and probing at 1000 nm. A NIR TA difference profile (Panel B) was constructed by subtracting the NIR TA kinetic obtained after transition to darkness from that obtained under steady-state illumination. Yellow bar: steady-state actinic illumination; Black bar: darkness following steady-state actinic illumination.

Figure 7. CT quenching in minor complexes as a function of EET from LHCII. Estimates of CT quenching in minor complexes and excitation energy transfer (EET) from excited LHCII to a quenching site in the minor complexes were estimated for isolated thylakoids (see text). The open and closed symbols represent data that are based on the assumption of 50% and 0% singlet-singlet annihilation in minor complexes, respectively. Horizontal, hatched bar corresponds to an estimate of Φ_{qE} (43%±5%) in isolated thylakoids used for the laser experiment.

Table 1. HPLC analyses of sucrose gradient Bands 2 and 3 from wild type and *npq*2. Pigment numbers are on a per 100 chlorophyll basis. V: violaxanthin; A: anteraxanthin; Lut: Lutein; and Z: zeaxanthin

Sample	**V**	**A**	**Lut**	**Z**
Wt B2	5.2	0.0	11.5	0.0
Wt B3	3.2	0.0	15.5	0.0
***npq2* B2**	0.0	0.0	10.7	9.3
***npq2* B3**	0.0	0.0	16.2	6.6

Table 2. **Transient absorption time constants and amplitudes of monomeric complexes**. Pump at 650 nm, probe at 1000 nm.

	MLHC-V	MLHC-Z	Difference
τ_r / ps	-	2.9 ± 0.3	5.2 ± 0.7
τ_1 / ps	60 ± 3 (49%)	69 ± 7 (35%)	238 ± 22
τ_2 / ps	1087 ± 61 (51%)	358 ± 31 (65%)	-

Table 3. Transient absorption time constants and amplitudes of LHCII-V and -Z complexes. Pump at 650 nm, probe at 1000 nm.

	LHCII-V	LHCII-Z
τ_1 / ps	43 ± 2 (49%)	67 ± 7 (46%)
τ_2 / ps	799 ± 49 (51%)	954 ± 130 (54%)

Table 4. **Title: R. Bassi please.** Chl: chlorophyll; Neo: neoxanthin; V: violaxanthin; A: anteroxanthin; Z: zeaxanthin; and Car: carotenoid.

sample	# Chl	Chl a/b	Chl /car	Neo	V	A	Lut	Z	Beta carotene	Car Total
Lhcb1-Z	12.0	1.5	5.1	0.0	0.0	0.0	1.4	1.0	0.0	2.4
Lhcb2-Z	12.0	1.5	5.2	0.0	0.0	0.0	1.3	1.0	0.0	2.3
Lhcb3-Z	12.0	1.5	5.1	0.0	0.0	0.0	1.4	1.0	0.0	2.4
Lhcb1-V	12.0	1.4	3.8	0.8	0.3	0.0	2.0	0.0	0.0	3.1
Lhcb2-V	12.0	1.4	3.8	0.8	0.3	0.0	2.0	0.0	0.0	3.2
Lhcb3-V	12.0	1.4	3.8	0.7	0.4	0.0	2.1	0.0	0.0	3.2

Table 5. **Fluorescence decay lifetime constants and amplitudes of monomeric complexes.** Excitation at 650 nm, detection at 690 nm.

Time \ Sample	MLHC-V	MLHC-Z
0.073 ns	11.6%	10.1%
0.63 ns	8.8%	22.8%
2.18 ns	27.0%	32.9%
4.14 ns	52.6%	34.2%
Φ_F^*	1.00	0.82

*Relative fluorescence quantum yield = $\Phi/\ \Phi_F$(MLHC-V)

Table 6. **Fluorescence decay lifetime constants and amplitudes of LHCII trimeric complexes.** Excitation at 650 nm, detection at 690 nm.

Time \ Sample	LHCII-Vx	LHCII-Zx
0.60 ns	10.6%	10.6%
2.5 ns	30.7%	55.5%
3.9 ns	58.7%	33.9%
Φ_F^*	1.00	0.89

*Relative fluorescence quantum yield = $\Phi/\ \Phi_F$(LHCII-V)

Table 7. **Transient absorption time constants and amplitudes of *A. thaliana* thylakoids**. Pump at 650 nm, probe at 1000 nm.

Time \ sample	Quenched (light on)	Unquenched (light off)	Quenched-Unquenched
τ_{rise} / ps	-	-	10
τ1 / ps	134 ± 16 (100%)	10 ± 5 (42%)	133
τ2 / ps	N.D.	134 ± 17 (58%)	
τ_{avg} / ps	134	81	

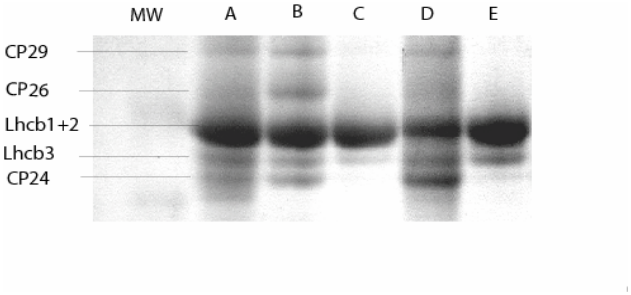

Figure 1

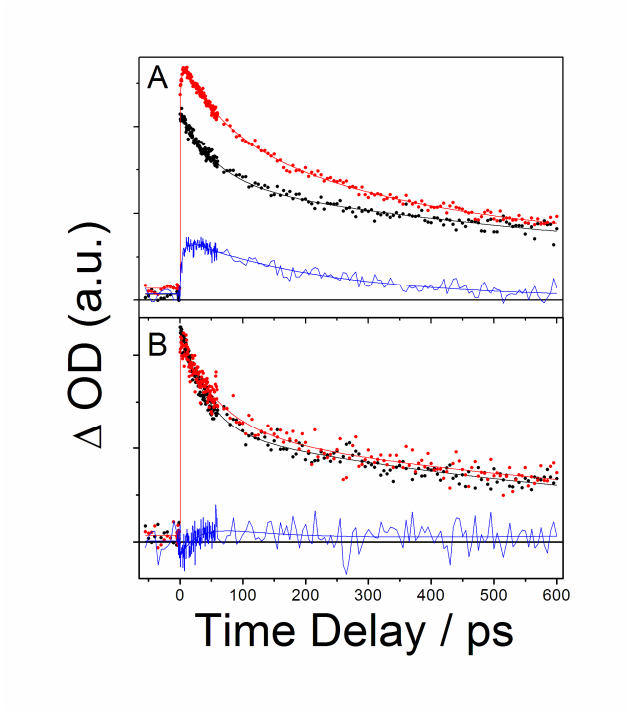

Figure 2

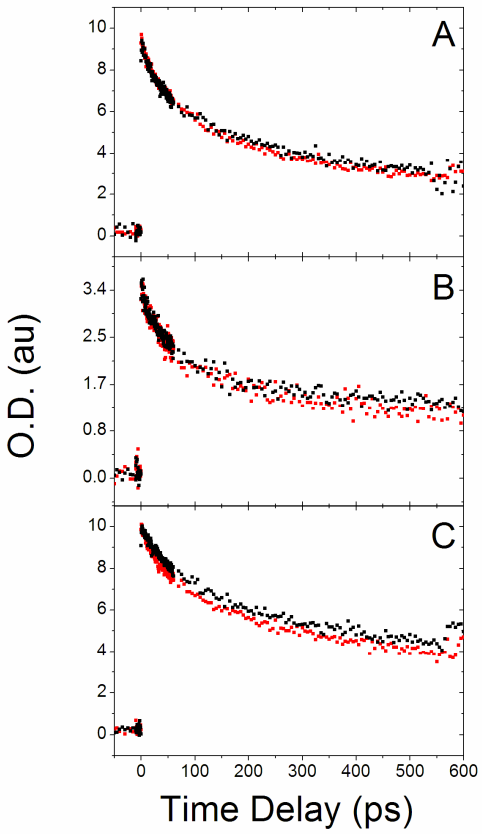
A
B
C
O.D. (au)
Time Delay (ps)
10
8
6
4
2
0
3.4
2.5
1.7
0.8
0.0
0
100
200
300
400
500
600

Figure 3

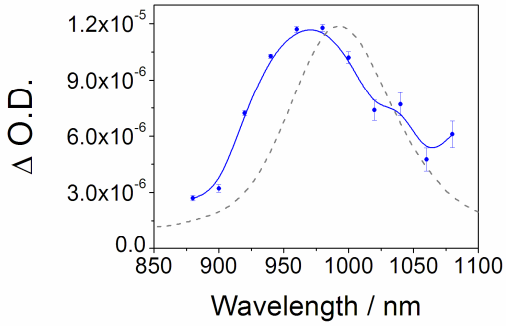
1.2x10-5
9.0x10-6
6.0x10-6
3.0x10-6
0.0
Δ O.D.
850
900
950
1000
1050
1100
Wavelength / nm

Figure 4

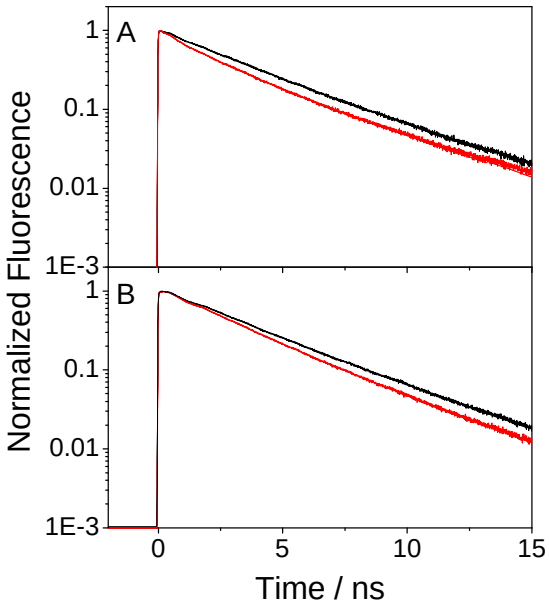

Figure 5

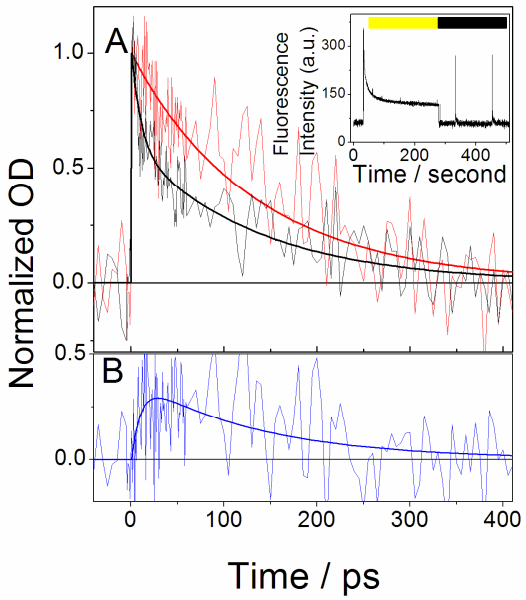
A
B
Normalized OD
1.0
0.5
0.0
0.5
0.0
0
100
200
300
400
Time / ps
Fluorescence Intensity (a.u.)
300
150
0
0
200
400
Time / second

Figure 6

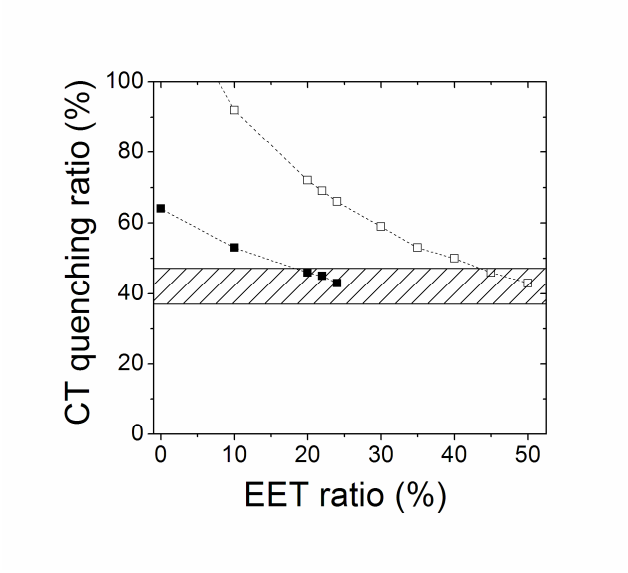

Figure 7